Ultrathin phase-inversion induced co-assembly separator for high-performance lithium-metal battery

Yuying Wang [a], Fanjun Guo [a], Mengzhen Zhou [a], Qian Wu [a], Tao You [a], Zhengxiang Zhong [a], Jiankun Yang [a], Li Liu [a], Yudong Huang [a*], Mingqiang Wang [a*]

[a] *School of Chemistry and Chemical Engineering, Harbin Institute of Technology, Harbin 150001, P. R. China.*

[*] Corresponding author: Yudong Huang. E-mail: huangyd@hit.edu.cn;
[*] Corresponding author: Mingqiang Wang. E-mail: mqwang@hit.edu.cn.

Experimental section

Synthesis of Holey GO and MPS-HGO

GO (Fig.S1) was prepared by the modified Hummers method.[1] Typically, $K_2S_2O_8$ (20 g) and P_2O_5(20 g) were added to concentrated sulfuric acid (100 ml), after completely dissolved by mechanical stirring, graphite powder (20 g) was slowly added and then heated to 80°C for 4.5 hours. After that, the resultant was cooled to room temperature and cleaned with deionized water to neutral, then dried at 80 °C to obtain pre-oxidized graphene. graphite powder (10 g) was added to concentrated sulfuric acid (230 ml) and placed in an ice bath to cool to 0°C, $KMnO_4$ (30 g) was slowly added and then the reaction system was heated to 35 °C for 2 hours, after that, 1 L of deionized water was slowly added in the mixture and heated to 90°C for 1 hours, and 25 ml of H_2O_2 was slowly added. After completion, slowly added H_2O_2 (25 ml) to the mixture solution gradually transforming it into a golden-yellow color. After stationing, the precipitate was removed and washed with deionized water to a pH value close to 6, and the product was dialyzed with deionized water to neutral to obtain a graphene oxide aqueous dispersion.

The holey GO (Fig.S2) was prepared as previously reported,[2] Briefly, the graphene oxide aqueous dispersion (2 mg ml^{-1}) was mixed with H_2O_2 (5 ml). Then the mixture was stirred at 100 °C for 4 hours to form nanopores on the GO surface. After the reaction, the collected solution was washed with deionized water and diluted into 2 mg mL^{-1}.

The MPS-HGO (Fig.S3) was synthesized by chemical grafting of silane coupling agents (Fig.S4). KH-570 (1 g) was added to ethanol (1 g) and stirring until dissolved thoroughly. Then added 50ml HGO (2 mg mL^{-1}) water dispersion, the mixture was sonicated for 30 min to ensure uniform dispersion. After adjusting the pH to 4~5 with

HCl, the mixture was stirred at 70 °C for 4 hours. The product was washed by centrifugation to remove the unreacted silane coupling agent and freeze-dried.

Synthesis of MA-POSS

The MA-POSS was prepared according to the next steps (Fig.S5). TMAH (0.65 g) and deionized water (13 ml) was added to a mixture of acetone and xylene (volume ratio is 1:1), after stirring until completely dissolved, KH-570 (60 g) was slowly added and then the mixture was stirred for 2 days at 40 ℃. After the reaction, an equal volume deionized water was added, stillness allowed for the division of the system. Then the upper layer was separated, rinsed again with v deionized water to neutralize the solution's pH. The product is obtained by rotary evaporation and concentration. Mass spectrometry characterization (Fig.S6) and FTIR (Fig.S7) spectrum proved the alkylation of POSS is successful.

Preparation of the MPMGA Separators

The ANF was prepared based on the previous method.[3] Kevlar fiber (1 g) and KOH (1.5 g) were added into DMSO (100 g) solution, and the mixture was stirred for 4 days at 55 ℃ to obtain dark red solution. To prepare MPS-HGO/ANF membranes, MPS-HGO was dissolved into the DMSO solution of ANF with mass fractions of 5%, 10%, 20% and 30%. Next, the mixture was applied to a glass plate with a film applicator at a thickness of 250 nm and immersed in deionized water for a phase conversion self-assembly process. Then the composite membranes were soaked and washed in DMSO, and immersed it in a DMSO solution containing 5wt% MA-POSS and 1wt% TPO polymerized by ultraviolet (365nm) irradiation. Finally, the composite films were spread on PTFE plate and placed it in an oven at 40 ℃ to dry obtaining MPMGA separators.

Characterization

Field emission scanning electron microscope (FE-SEM, SUPRA55) combined with energy dispersive X-ray spectroscopy (EDS) was used to characterize the surface morphology, cross-sectional morphology and elemental distribution of the separator, as well as the surface of lithium metal. Transmission Electron Microscope (TEM) images were obtained from JEM-2100, JEOL, Japan. X-ray photoelectron spectroscopy (XPS, AXISULTRA DLD) measurements were used to characterize the chemical

composition of the separator surface. The mechanical tests were conducted on a TA XT Plus Texture Analyzer (Stable Micro Systems Ltd.) with the test of longitudinal direction carried out at a rate of 1 cm min^{-1}. The membranes were cut into 10 mm × 5 mm and five samples were tested in each case.

The separator porosity is measured by the weights of the separator before and after the absorption of N-butanol as the following equation:[4]

$$P\% = \frac{W - W_0}{\rho V_0} \times 100\% \quad (1)$$

where W_0 and W represent the weights of the separator before and after immersing a liquid, respectively, ρ is the density of the N-butanol, and V_0 is the geometric volume of the separator.

Cell Assembly and Electrochemical Measurements

The electrochemical performance was evaluated using 2025-coin cells assembled in a glove-box (<0.1 ppm of oxygen and water). The carbonate electrolyte was composed of 1 mol L^{-1} LiTFSI in solution in EC/PC (v/v = 1/1), and the amount of electrolyte was controlled as 100 μL. The LFP electrodes were prepared by the conventional mixing-casting method, in which the mixture of active materials, acetylene black and PVDF (mass ratio of 7:2:1) in NMP was coated on aluminum foil followed by drying in a vacuum oven for 12 h. The average mass loading of LFP was≈4 mg cm^{-2}. The ultra-high LFP loading electrodes with 20 mg cm^{-2} were taken from the Canrd company. The charge/discharge cycling performance were tested on the Newear CT4008 battery-testing system. The electrochemical impedance spectra (EIS), the cyclic voltammetry (CV) and the linear scanning voltammetry (LSV) were implemented on electrochemical workstation (CHI660E), the EIS was carried out in the frequency range of 0.01Hz to 1 M Hz with stain less steel (SS)/separator/SS cell, the CV was performed from 2.5 to 4 V at scan rates of 0.1, 0.2,0.3, 0.5, 1 m V s^{-1} with LFP/separator/Li cell and the LSV was carried out from 1 to 5 V at a scan rate of 0.1 m V s^{-1} with SS/separator/Li cell.

The ion conductivity of separators was measured by the EIS analysis tested obtained from the equation:[5]

$$\sigma = \frac{d}{R \cdot S} \quad (2)$$

where σ is the ionic conductivity, d is the thickness of separator, R is the bulk resistance and S is the area of the SS electrodes.

The Li ion transference number was evaluated according to the following equation:[6]

$$t_{Li^+} = \frac{I_S(\Delta V - I_0 R_0)}{I_0(\Delta V - I_S R_S)} \quad (3)$$

where ΔV is the constant applied potential (10 mV), I_0 and I_s are the initial and steady-state current, R_0 and R_s are the interfacial resistance before and after polarization measured.

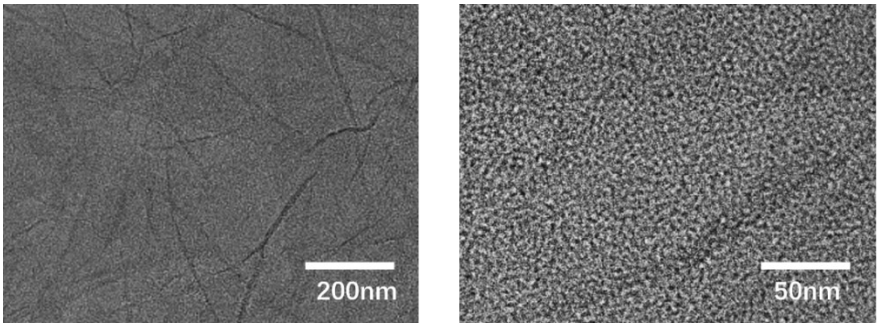

Fig.S1 TEM image of GO.

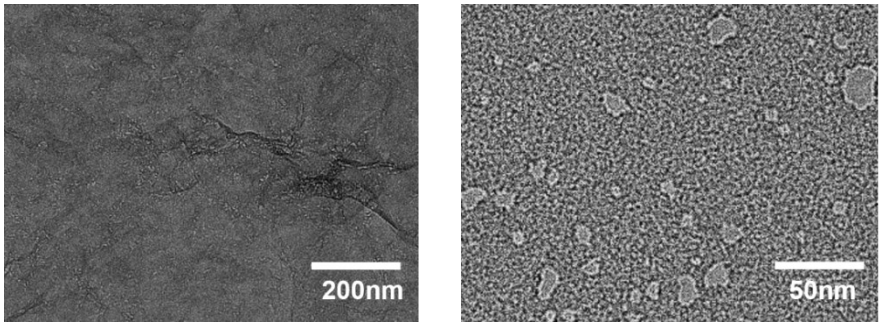

Fig.S2 TEM image of HGO.

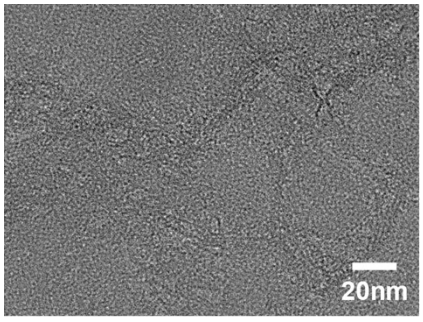

Fig.S3 TEM image of MPS-HGO.

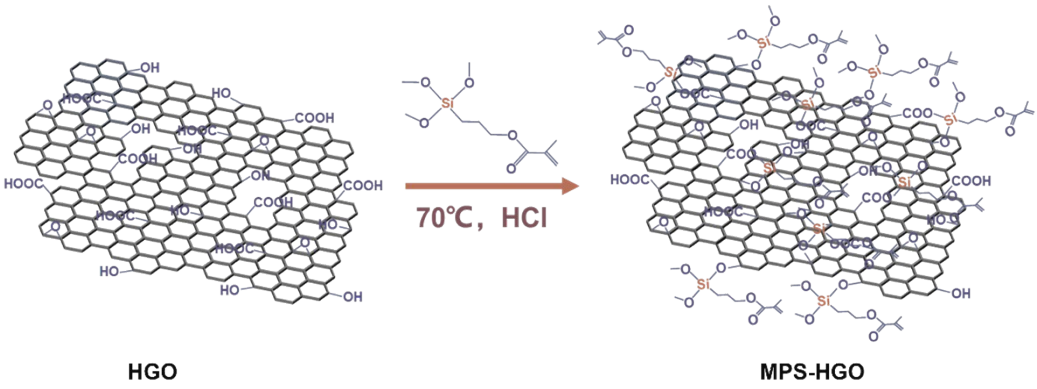

Fig.S4 Synthesis of MPS-HGO.

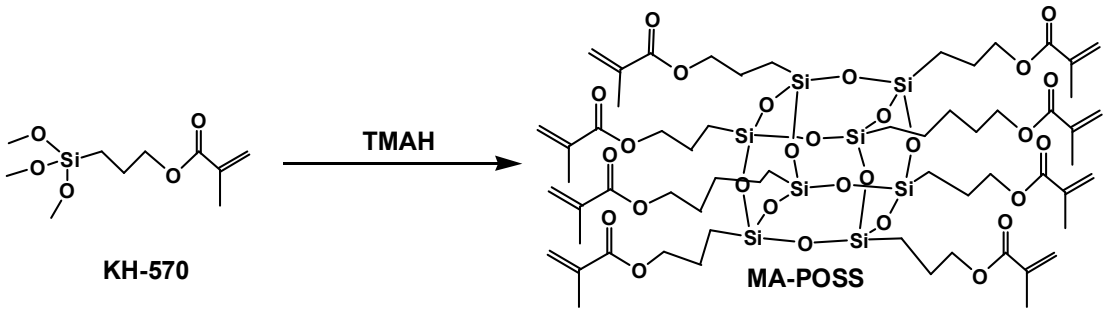

Fig.S5 Structure of MA-POSS.

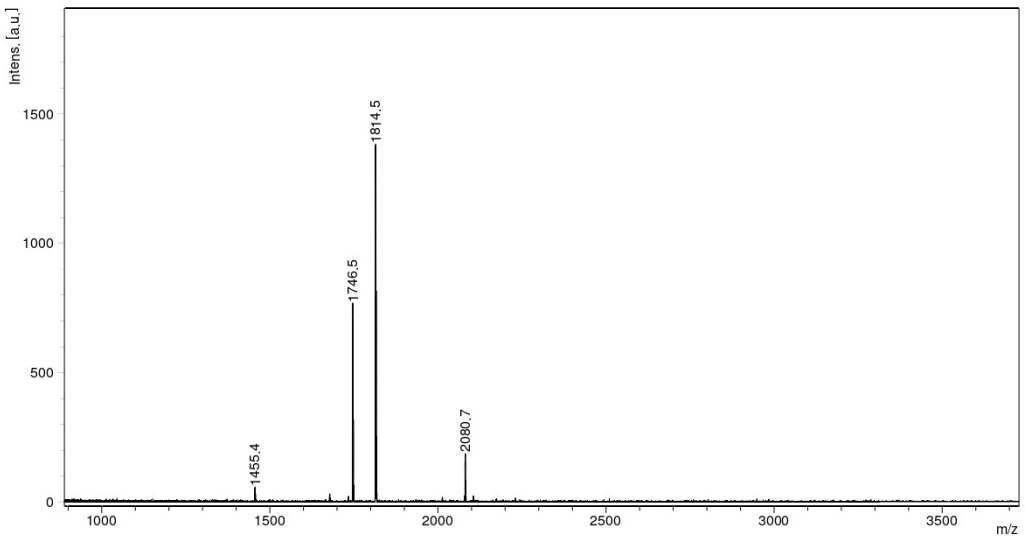

Fig.S6 Mass spectrometry characterization of MA-POSS.

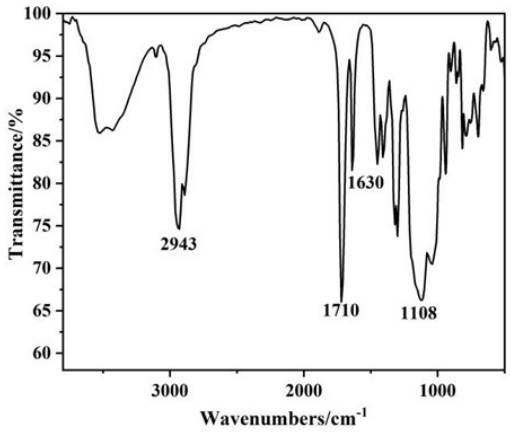

Fig.S7 FTIR spectrum of MA-POSS.

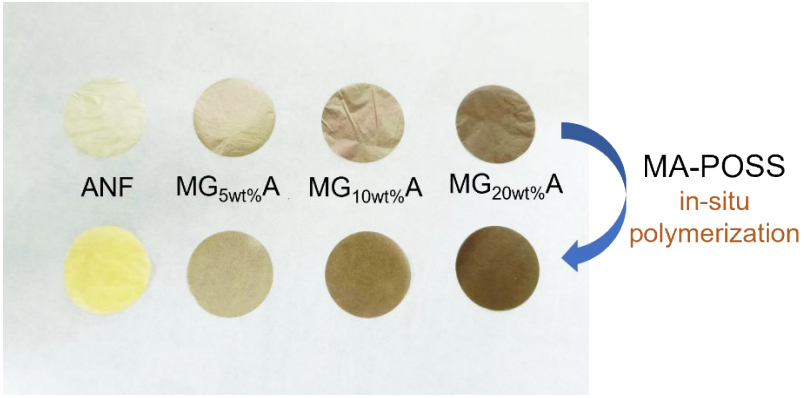

Fig.S8 Photos of the composite separators with various contents of HGO.

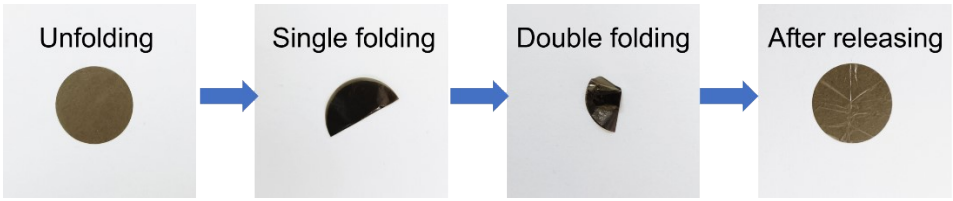

Fig.S9 Photos of the folding and releasing process of the MPMG$_{20wt\%}$A separators

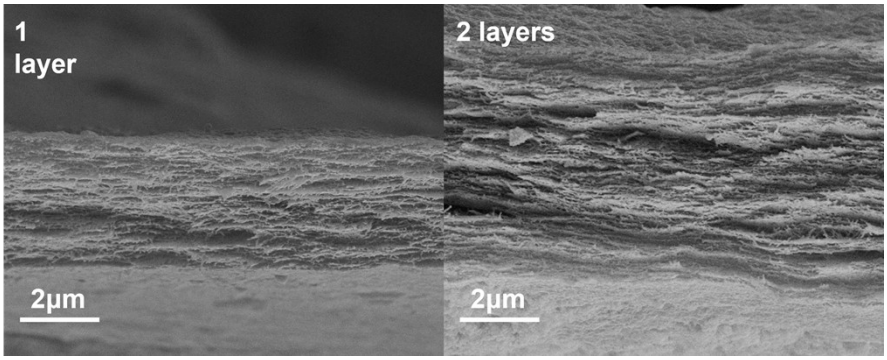

Fig.S10 SEM image of superimposed membranes.

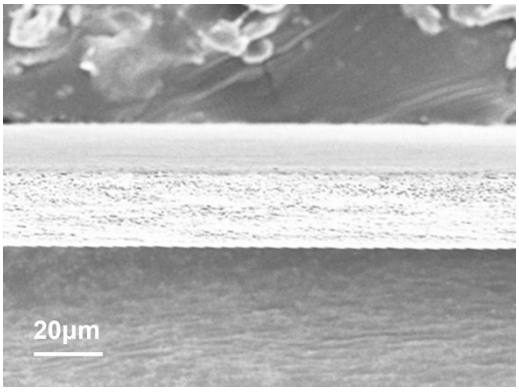

Fig.S11 SEM image of PE separators.

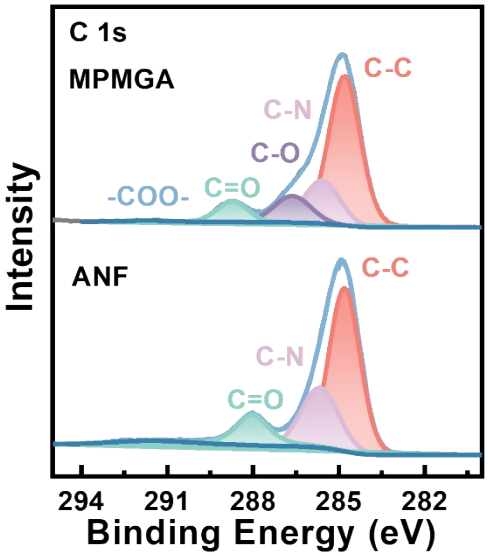

Fig.S12 C 1s XPS spectra of MPMGA and ANF separators.

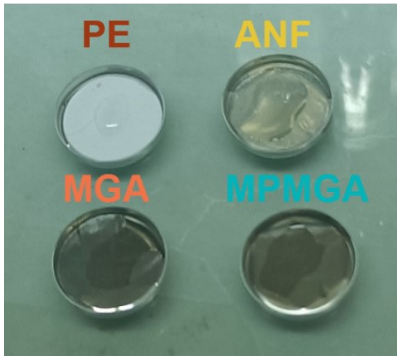

Fig.S13 Wettability of different separators.

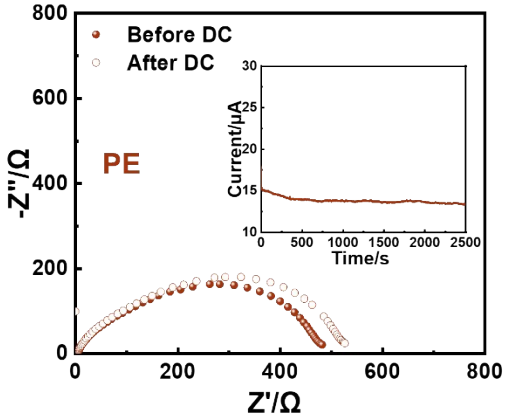

Fig.S14 AC impedance before and after polarization and Chronoamperometry profiles of PE separator.

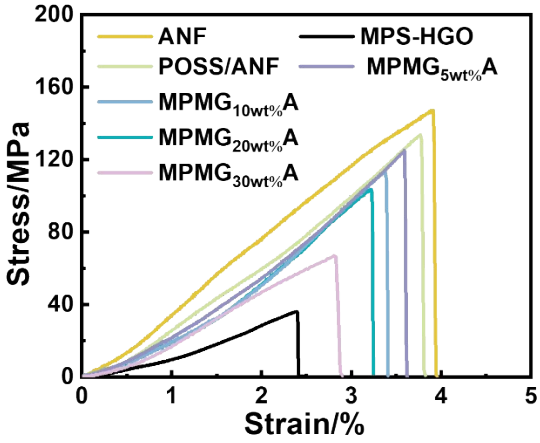

Fig.S15 Tensile strength of the composite separators with various contents of HGO.

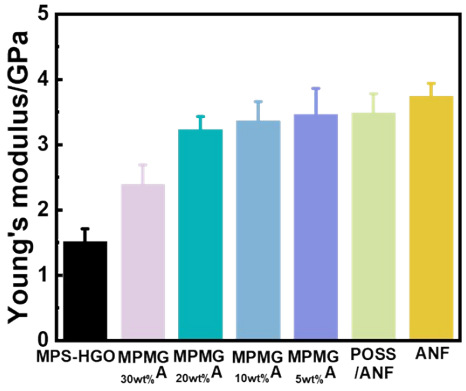

Fig.S16 Young's modulus of the composite separators with various contents of HGO.

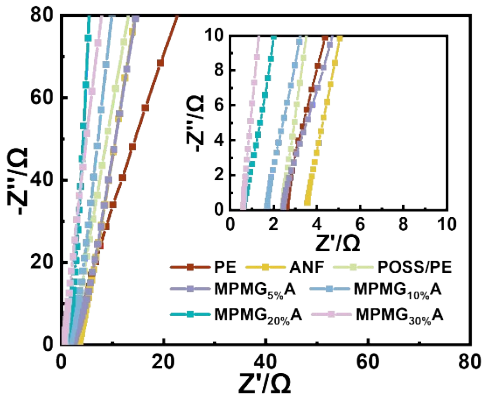

Fig.S17 EIS of the composite separators with various contents of HGO.

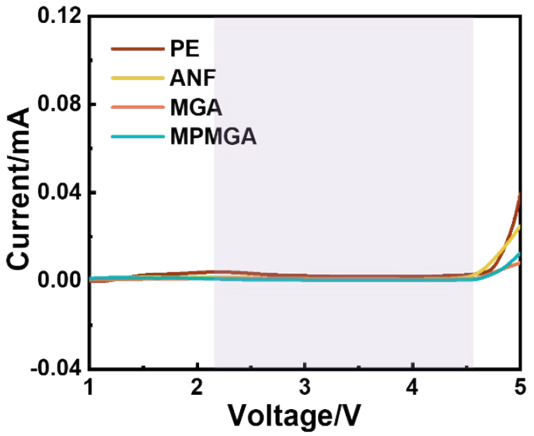

Fig.S18 The LSV curves of Li/separator/SS cells with different separators.

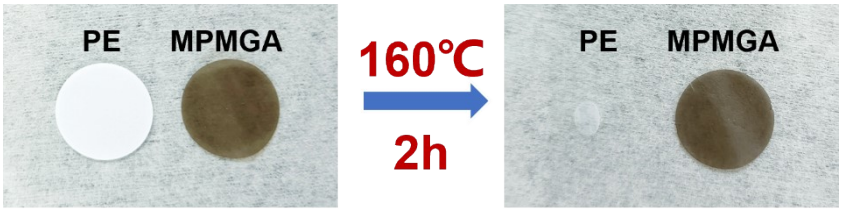

Fig.S19 Photos of different separators before after heat treated at 160℃ for 2 hours.

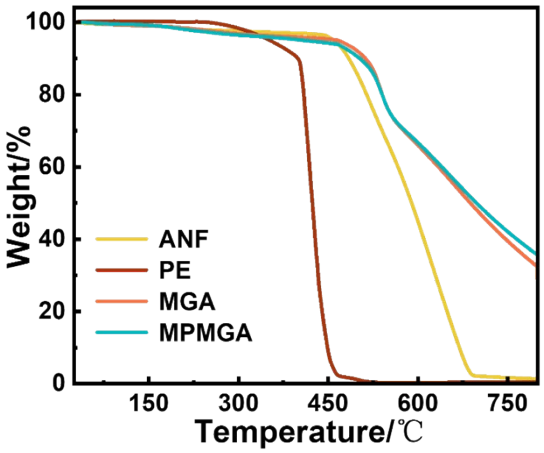

Fig.S20 Thermogravimetric analysis curves for different separators. The testing heating rate is 10 ℃ min^{-1} under the N_2 atmosphere.

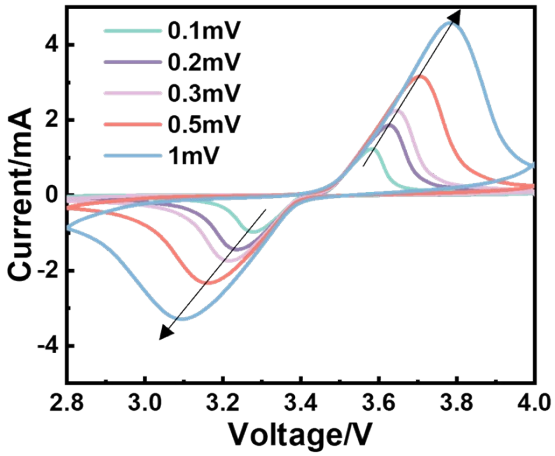

Fig.S21 CV curves of coin cells with MPMGA.

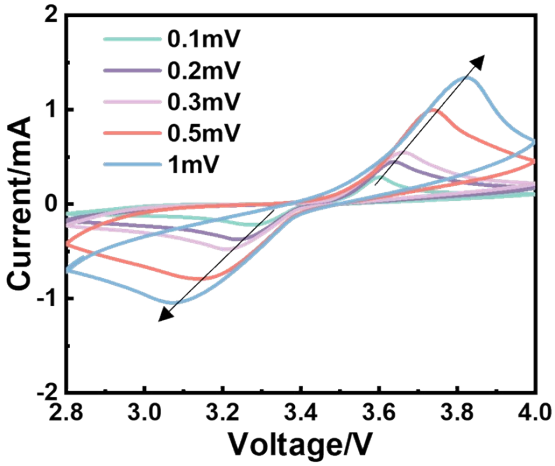

Fig.S22 CV curves of coin cells with PE.

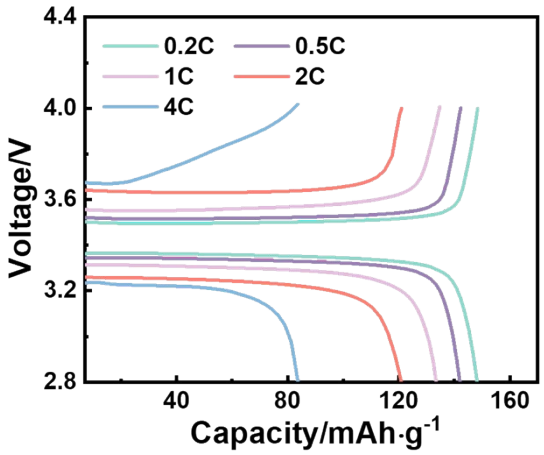

Fig.S23 First cycle charge-discharge curves of cells with PE.

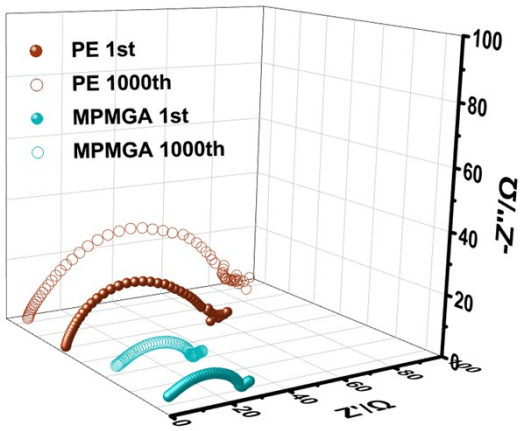

Fig.S24 Impedance performance changes over time of LFP/Li cells at 2C with different separators.

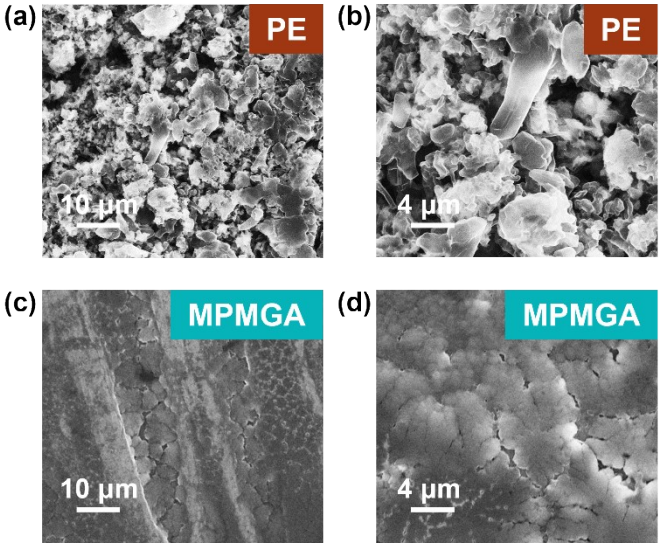

Fig.S25 SEM images of Li metal anodes in LFP/Li cells with different separators after cycling.

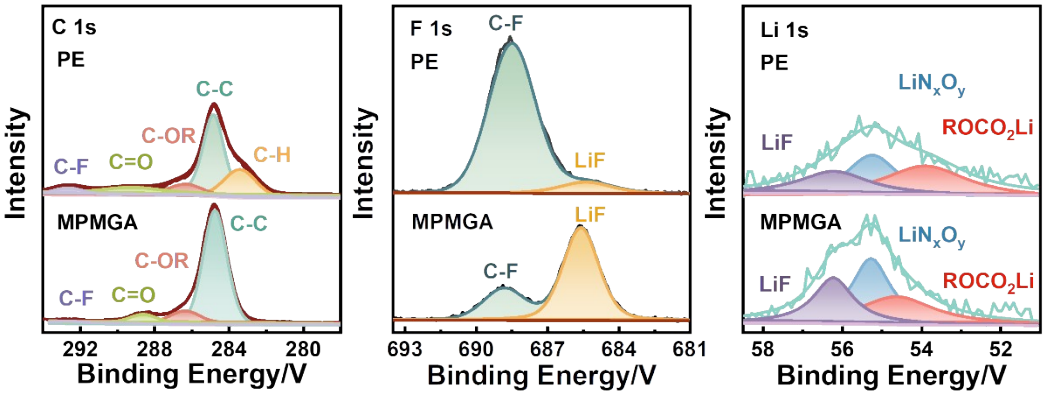

Fig.S26 XPS spectra of Li anode after cycling of LFP/Li cells with PE or MPMGA separators.

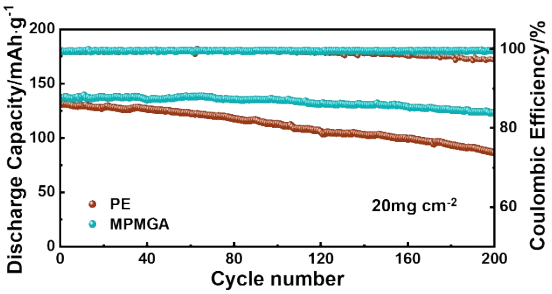

Figure S27 Cycling performances of cells at 0.5 C with a cathode mass loading of 20 mg cm^{-2}

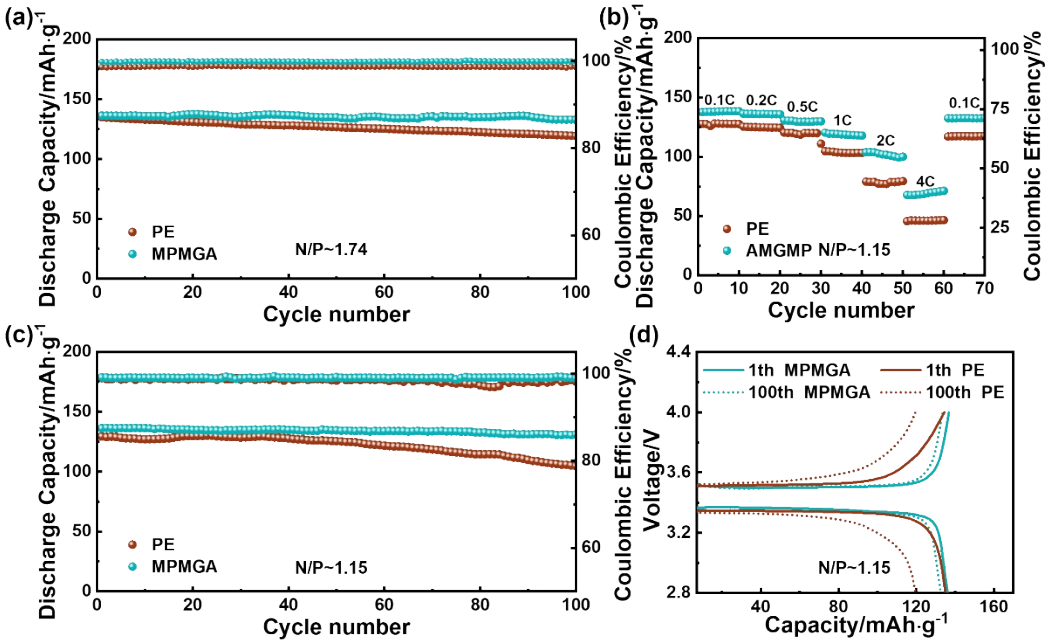

Fig.S28 (a) Cycling performances of LFP/Li cells with different separators (N/P ~1.74) at 0.5 C (b) Rate capability of LFP/Li cells with different separators (N/P ~1.15)
(c) Cycling performances of LFP/Li cells with different separators (N/P ~1.15) at 0.5 C
(d) Charge-discharge curves of LFP/Li cells with different separators (N/P ~1.15) at 0.5 C.

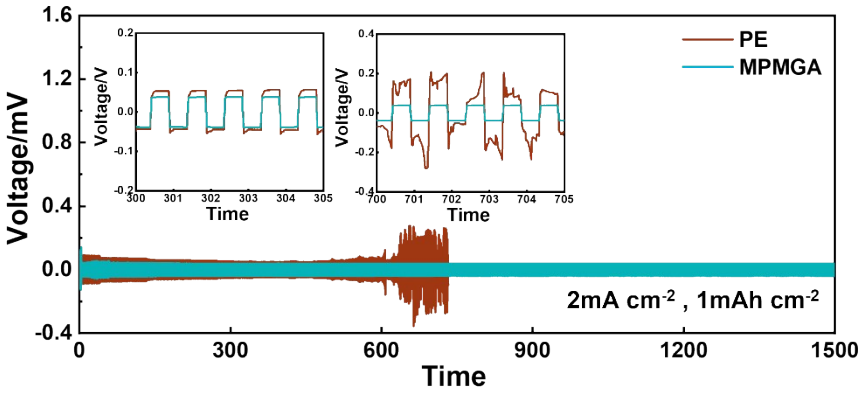

Fig.S29 Cycling performances of Li|Li symmetric cells with different separators at current densities of 3 mA cm^{-2} with a capacity of 3mAh cm^{-2}.

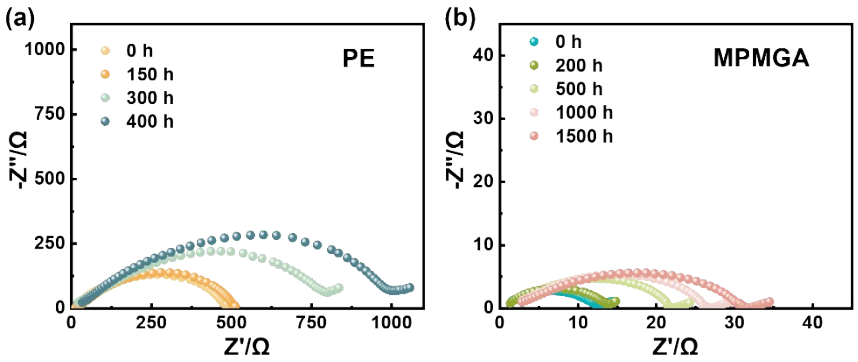

Fig.S30 Impedance spectroscopy for different cycles of Li|Li symmetric cells with different separators at current densities of 5 mA cm^{-2} with a capacity of 5 mAh cm^{-2}.

Table S1 Comparison of tensile strength, tensile modulus elongation at break, porosity and ionic conductivity of different separators

Separator	**Tensile strength (MPa)**	**Tensile modulus (GPa)**	**Porosity (%)**	**Ionic conductivity (mS cm^{-1})**
PE	54.92±3.3	0.14±0.022	60	0.36
ANF	147.3±3.8	3.74±0.1	28	0.08
MGA	114.9±4.4	3.21±0.12	52	0.2
MPMGA	104±5.1	3.23±0.2	71	0.41

Table S2 Comparison of electrochemical performance of the MPMGA with separators of related materials in publications in LMBs

Separator	**Cathode**	**LFP loading (mg cm^{-2})**	**Electrochemical Performance**				**REF**
			Initial discharge capacity (mAh g^{-1})	**Capacity fade per cycle (%)**	**Current density (1C = 170 mA g^{-1})**	**Number of cycles**	
MPMGA	*LFP*	*4*	*154*	*0.0016*	*0.5 C*	*250*	This work
CF/ANF	CNT/S	9	145	0.1096	0.5C	100	[7]
ANF/PP	LMO	4.2	~	0.041	0.5C	300	[8]
ANF/HAP/PP	LFP	3	145	0.064	0.5C	180	[9]
ZIF-8/ANF	LFP	9	148	0.093	0.5C	100	[10]
ANF/BC	LFP	3	157	0.064%	0.2C	100	[11]
PMIA/GO	LFP	~	145	0.077%	0.5C	50	[12]
PU/GO	LFP	4	155	0.044%	0.2C	300	[13]
TPP@PVDF/SiO_2/GO	LFP	~	150	0.05%	0.5C	50	[14]
GO/PVDF-HFP	LFP	3	150	0.084%	0.5C	30	[15]
HGO-PAN	LFP	1.37	141	0.005%	0.5C	900	[16]
POSS/PMIA	$LiCoO_2$	4	133	0.1096%	0.1C	100	[17]

Table S3 Comparison of electrochemical performance of the MPMGA with that of recent publications in LMBs with various separators

Separator Membrane	**Cathode**	**Electrochemical Performance**					**REF**
		Initial discharge capacity (mAh g^{-1})	**Capacity retention (%)**	**Capacity fade per cycle (%)**	**Current density (1C = 170 mA g^{-1})**	**Number of cycles**	
MPMGA	*LFP*	*141*	*85.7*	*0.0143*	*2C*	*1000*	This work
EAA	LFP	107	69	0.155	5C	200	[18]
CNT-PAA-Cu/IR	LFP	136	86.2	0.069	1C	200	[19]
DBDPE/CaO/DCPE	NCM811	191	80	0.1	0.5C	200	[20]
PVDF-MOF	LFP	148	81	0.076	1C	250	[21]
PBI-5M	LFP	150	76.6	0.047	2C	500	[22]
MIL-101（Cr）/PAN	NCM96	125	81	0.063	1C	300	[23]
TBAHP/PVDF-HFP-PMIA	$LiCO_2$	140	89.2	0.054	0.5	200	[24]
PMOF80-CE	LFP	135	85	0.0375	1C	400	[25]
TpPa-SO_3Li/PE	LFP	144	94.9	0.017	1C	300	[26]
PVDF/ZSM-Si (Al)/PE	LCO	140	94.5	0.055	0.2	100	[27]
L-SEI/PP	NCM	150	73.5	0.265	0.4C	100	[28]
HMSS/PP	LFP	135	90	0.04	1C	250	[29]
APP/ZIF-8/PP	LFP	136	96.1	0.04	1C	100	[30]
PDA/AlN/PP	LFP	120	89	0.022	3C	500	[31]
MAF-6/PP	LFP	140	73.2	0.0179	1C	1500	[32]
LiPON /PP	LFP	142	92	0.0145	0.5C	550	[33]
DMS/PP	LFP	120	85	0.015	1C	1000	[34]

REFERENCES

1 G. Zhang, W. Li, Z. Chen, J. Long, C. Xu, *Carbon.*, 2022, **187**, 86-96.

2 Y. Xu, C. Chen, Z. Zhao, Z. Lin, C. Lee, X. Xu, C. Wang, Y. Huang, M.I. Shakir, X. Duan, *Nano Lett.*, 2015, **15**, 4605-4610.

3 B. Yang, L. Wang, M. Zhang, J. Luo, Z. Lu, X. Ding, *Adv. Funct. Mater.*, 2020, **30**, 2312132.

4 J. Seo, J. Im, M. Kim, D. Song, S. Yoon, K.Y. Cho, *Small.*, 2024, e2312132.

5 Y. Liu, Z. Tai, I. Rozen, Z. Yu, Z. Lu, A.P. LaGrow, O. Bondarchuk, Q. Chen, G. Goobes, Y. Li, L. Liu, *Adv. Energy Mater.*, 2023, **13**,2204420.

6 D. Lee, A. Jung, J.G. Son, B. Yeom, *Energy Storage Mater.*, 2023, **61**, 102902.

7 S. Zhang, J. Luo, M. Du, H. Hui, Z. Sun, *Eur. Polym. J.*, 2022, **171**, 111222.

8 S. Hu, S. Lin, Y. Tu, J. Hu, Y. Wu, G. Liu, F. Li, F. Yu, T. Jiang, *J. Mater. Chem. A*., 2016, **4**, 3513-3526.

9 B. Yang, R. Pang, J. He, H. Sun, B. Yuan, M. Zhang, *J. Power Sources.*, 2024, **600**, 234259.

10 S. Zhang, J. Luo, F. Zhang, X. He, *Compos. Commun.*, 2022, **32**, 101183.

11 Y. Chen, J. Li, Y. Ju, R. Cheng, Y. Zhai, J. Sheng, H. Liu, L. Li, *Appl. Surf. Sci.*, 2022, **592**, 153222.

12 X. Wang, H. Zhao, N. Deng, Y. Li, R. Yu, Y. Wen, W. Kang, B. Cheng, *Sustain. Energ. Fuels.*, 2022, **6**, 386-397.

13 W. Lu, Z. Yuan, Y. Zhao, H. Zhang, H. Zhang, X. Li, *Chem. Soc. Rev.*, 2017, **46**, 2199-2236.

14 M. Waqas, S. Ali, C. Feng, D. Chen, J. Han, W. He, *Small.*, 2019, **15**, e1901689.

15 A. L. Ahmad, U. R. Farooqui, N. A. Hamid, *RSC Adv.*, 2018, **8**, 25725-25733.

16 Y. Chen, J. Li, Y. Ju, R. Cheng, Y. Zhai, J. Sheng, H. Liu, L. Li, *Appl. Surf. Sci.*, 2022, **592**, 153222.

17 J. Ma, X. Ma, H. Zhang, F. Chen, X. Guan, J. Niu, X. Hu, *J. Membr. Sci.*, 2022, **659**, 120811.

18 Y. Chen, P. Mickel, H. Pei, Y. Wen, X. Guan, Y. Wang, X. Wang, O.A. Mhtachem, C. Zhang, H. Nie, X. Zhou, P. Kral, X. Xie, *ACS Appl. Mater. Interfaces.*, 2023, 15, 18333-18342.

19 R. Li, Y. Peng, P. Li, X. Hu, *Chem. Eng. J.*, 2024, **479**, 147559.

20 J. H. Yang, Y.K. Jeong, W. Kim, M.A. Lee, J.W. Choi, H.S. Kim, K.J. Kim, *Adv. Energy Mater.*, 2024, 2304366.

21 M. Li, S. Cheng, J. Zhang, C. Huang, J. Gu, J. Han, X. Xu. *Chem. Eng.*, *J.* 2024,**487**, 150709.

22 A. Hussain, W. Raza, A. Mehmood, S. Jalees, L. Ao, Y. Deng, A. Ramiere, X. Cai, D. Liu, *J. Energy Chem.*, 2024, **94**, 288-298.

23 S. Wang, Y. Yu, S. Fu, H. Li, J. Huang, *J. Energy Chem.*, 2024, **92**, 132-141.

24 H. Zhao, N. Deng, W. Kang, Z. Li, G. Wang, B. Cheng, *Energy Storage Mater.*, 2020, **26**, 334-348.

25 Z. Li, Q. Liu, L. Gao, Y. Xu, X. Kong, Y. Luo, H. Peng, Y. Ren, H. B. Wu, *J. Energy Chem.*, 2021, **52**, 354-360.

26 G. Yu, Y. Cui, S. Lin, R. Liu, S. Liu, Y. Zhu, D. Wu, *Adv. Funct. Mater.*, 2024, 2314935.

27 X. Mao, L. Shi, H. Zhang, Z. Wang, J. Zhu, Z. Qiu, Y. Zhao, M. Zhang, S. Yuan, *J. Power Sources.*, 2017, **342**, 816-824.

28 J. Liu, R. Xu, C. Yan, H. Yuan, J. Ding, Y. Xiao, T. Yuan, J. Huang, *Energy Storage Mater.*, 2020, **30**, 27-33.

29 J. Si, X. Li, N. Ren, H. He, S. Zeng, C. Chen, *J. Power Sources.*, 2024, **599**, 234225.

30 D. Li, Y. Ouyang, Y. Xiao, Y. Xie,Q. Zeng, S. Yu, C. Zheng, Q. Zhang, S. Huang, *Adv. Funct. Mater.*, 2024, 2314296.

31 W. Tang, T. Zhao, K. Wang, T. Yu, R. Lv, L. Li, F. Wu, R. Chen, *Adv. Funct. Mater.*, 2024, 2314045.

32 W. Wu, Y. Xu, X. Ke, Y. Chen, Y. Cheng, G. Lin, M. Fan, L. Liu, Z. Shi, *Energy Storage Mater.*, 2021, **37**, 387-395.

33 Y. Pang, M. Guan, Y. Pan, M. Tian, K. Huang, C. Jiang, A. Xiang, X. Wang, Y. Gong, Y. Xiang, X. Zhang, *Small.*, 2022, 182104832.

34 W. Ren, K. Zhu, W. Zhang, H. Liang, L. Xu, L. Wang, C. Yang, W. Yang, P. Zhang, F. Wang, Y. Wang, W. Li, *Adv. Funct. Mater.*, 2023, **33**, 2301586.